Simulation and Experimental Study of the Optical Properties of Black Silicon Synthesized by Reactive Ion Etching

Gagik Ayvazyan
National Polytechnic University of Armenia, Yerevan, Armenia
agagarm@gmail.com (corresponding author)

Arthur Aghabekyan
National Polytechnic University of Armenia, Yerevan, Armenia
artag@inbox.ru

Received: 21 November 2025 | Revised: 23 December 2025 | Accepted: 3 January 2026

 DOI: https://doi.org/10.48084/etasr.16409

ABSTRACT

This work presents a combined numerical and experimental study of the optical properties of black Silicon (b-Si), which is synthesized by reactive ion etching. Finite-Difference Time-Domain (FDTD) simulations based on a periodic nanocone model were used to analyze how nanostructure geometry influences spectral absorption, reflectance, and transmittance. The modeling results show that nanocone heights in the range of 650-700 nm and dense packing conditions, where the base diameter approaches the periodicity, provide optimal broadband antireflection. Experimental measurements confirm a reduction of the average reflectance to below ~2–3% in the visible range (400-700 nm) for b-Si layers with heights around 670 nm, in good agreement with simulation trends. The results establish quantitative geometric design rules for the targeted fabrication of broadband antireflective silicon surfaces and demonstrate the potential of b-Si for applications in silicon solar cells, photodetectors, and other optoelectronic devices.

Keywords-black silicon; solar cell; optical properties; morphology; FDTD simulation

I. INTRODUCTION

Although silicon is the basic material used in microelectronics and photovoltaics, having high reflectivity (30-40% in the visible spectrum) significantly reduces the efficiency of solar cells by minimizing light absorption. Conventional antireflection strategies, such as micron-scale pyramidal texturing [1, 2] or single-layer dielectric coatings [3, 4], offer limited spectral and angular performance. On the other hand, methods, such as porous silicon layers [5, 6] or multilayer coating stacks [7], improve broadband response but often have cost, stability, and scalability issues. Furthermore, most of these techniques rely on wet-chemical processing, which is undesirable for modern microelectronic manufacturing. b-Si has emerged as a promising platform for broadband, angle-insensitive antireflection surfaces [8, 9], featuring a dense array of nanoscale surface structures, typically ranging in height from several hundred nanometers to a few micrometers. Low reflectance comes from a continuous effective refractive index gradient between air and silicon, which is formed by the depth-dependent filling fraction within the nanostructured layer. This gradient, combined with enhanced multiple scattering and light-trapping effects, allows b-Si surfaces to achieve reflectance levels below 2% across a broad spectral range [10, 11]. Reactive Ion Etching (RIE) is a technique that provides a highly controllable, dry method for producing b-Si, by balancing chemical etching with fluorine-containing ions and surface oxidation through the formation of a stable oxyfluoride layer. Adjusting plasma chemistry, chamber pressure, RF power, and etching duration carefully enables precise control over the morphology and optical performance of the resulting nanostructures. Despite significant progress in b-Si fabrication, creating clear, quantitative correlations between RIE process parameters, surface morphology, and the resulting optical response is still a major challenge. Numerical modeling provides an effective framework for addressing this issue by enabling the predictive optimization of nanostructure geometry without the need for extensive experimental iteration. The FDTD method is an accurate tool for modeling light-matter interactions in complex nanostructured media because it directly solves Maxwell's equations in the time domain and captures key phenomena, such as diffraction, scattering, and near-field effects [12]. This work aims to examine the optical properties of b-Si synthesized by RIE using a combined approach of FDTD simulations and experimental characterization. Unlike our previous studies summarized in [8], this work creates explicit, quantitative correlations between the geometric parameters of b-Si and its broadband optical response. These correlations are consistently validated by modeling and experimentation, providing practical

criteria for fabricating nanostructured layers with optimized antireflection performance for use in silicon solar cells, photodetectors, and other optoelectronic devices.

II. SAMPLE PREPARATION AND CHARACTERIZATION

The initial substrates were p-type, boron-doped, single-crystal silicon (Si) wafers with a (100) orientation and a resistivity of 1.0–3.0 Ω·cm. Prior to processing, the wafers underwent a standard chemical cleaning procedure to ensure the complete removal of organic, ionic, and native oxide contaminants. This procedure consisted of sequential treatments in acetone, isopropanol, and diluted Hydrofluoric (HF) acid. The b-Si layer was synthesized using RIE in a modified "Plasma 600" plasma etching system. The plasma was generated using an RF generator operating at the standard industrial frequency of 13.56 MHz in a gaseous mixture of sulfur hexafluoride (SF6) and oxygen (O2). The base etching process was defined by the following parameters: an RF discharge power of 100 W, a chamber pressure of 60 mTorr, and a gas flow ratio of SF6/O2 = 2:1. This corresponds to absolute flow rates of 75–80 sccm for SF6 and 35–40 sccm for O2, respectively. To examine the kinetics of nanostructure growth and its impact on optical properties, the etching time was systematically varied from 3 min to 15 min, preparing 3 samples. The surface and cross-sectional morphologies of the b-Si samples were examined using a Philips XL 40 Scanning Electron Microscope (SEM). This enabled direct measurement of the nanostructure height, base diameter, and surface density. Optical characterization was performed in the spectral range of 250–1150 nm using a Shimadzu UV-3101PC spectrophotometer equipped with an integrated sphere. This setup reliably separates the specular and diffuse components of reflected and transmitted light. The optical spectra were recorded with a 1-nm wavelength step, a ±0.5-nm wavelength accuracy, and a ±0.3%-better-than-photometric accuracy. Directly recorded spectra included diffuse reflectance (R) and total transmittance (T). Absorption spectra (A) were subsequently calculated based on the energy conservation principle:

$$A = 100\% - R - T \quad (1)$$

Numerical modeling of the optical properties of the nanostructures, was performed, using Lumerical FDTD Solutions, a commercial software package widely recognized in the scientific community for solving electromagnetic problems in complex media [13]. The software offers high computational performance, an advanced graphical user interface, and integrated functions for near- and far-field analysis, making it a powerful tool for designing and optimizing photonic and plasmonic structures [14, 15], and was used to examine the antireflective properties of b-Si passivated by thin metal-oxide films [16]. The simulations allowed the variation of the key geometric parameters of the b-Si nanostructures (height, diameter, and periodicity) and their influence on the absorption and reflection coefficients, creating a quantitative link between morphology and optical response.

III. RESULTS AND DISCUSSION

A. Modeling

The first step in the numerical analysis was constructing a geometric model that could accurately represent the morphology of the fabricated b-Si layer. SEM images of surface and cross-sectional views, shown in Figure 1, revealed a highly irregular, randomly distributed array of high-aspect-ratio nanoneedles with significant variation in height, base diameter, and interspacing. In order to capture the essential optical behavior of such a stochastic surface while ensuring computational tractability, the real morphology by an ensemble of nanocones was approximated.

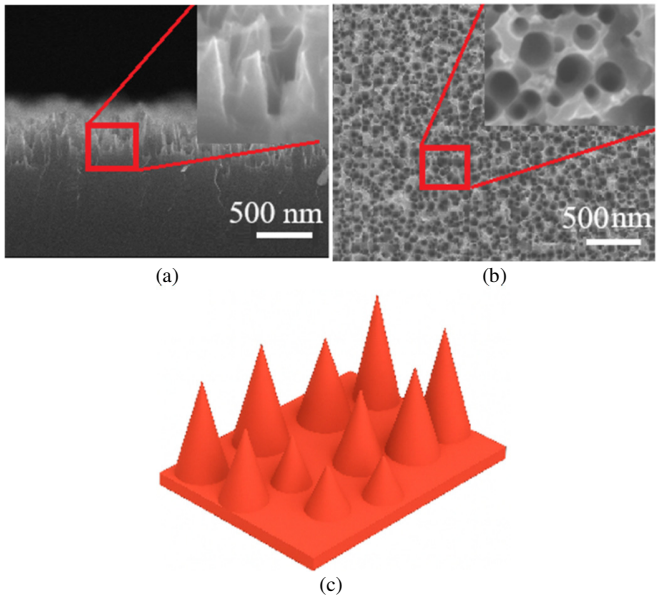

Fig. 1. (a) Cross-sectional and (b) top-view SEM images of b-Si (insets: 10× magnification); (c) 3D view of the stochastic cone-based model.

A simplified regular periodic model consisting of hexagonally arranged nanocones with average geometric parameters, such as cone height (h), base diameter (d), and lattice periodicity (t), was adopted for systematic parametric analysis, as depicted in Figure 2. The computational domain included one unit cell with one nanocone on a silicon substrate, while periodic boundary conditions were applied along the x and y directions to model an infinite array. The top and bottom boundaries were terminated with perfectly matched layers to prevent unphysical reflections. Light was provided by a normally incident broadband plane wave. Power monitors placed above the structure and beneath the substrate recorded the reflected and transmitted electromagnetic fluxes, enabling the extraction of wavelength-dependent optical coefficients. The optical constants for crystalline silicon, were taken from datasets to ensure consistency between simulation and reality. Mesh refinement was applied near the nanocone tip and sidewalls to accurately capture nanoscale field variations and scattering processes. The periodic nanocone model is an effective approximation of the real stochastic morphology, capturing the dominant optical mechanisms while neglecting local randomness in cone dimensions and spacing.

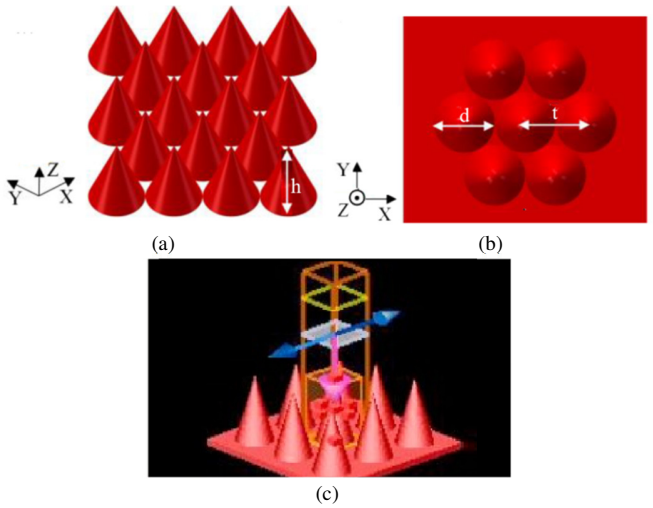

Fig. 2. (a) 3D and (b) 2D views of the regular periodic model, (c) computational domain.

The parametric analysis revealed clear dependencies of the optical response on the nanostructure geometry. Figure 3 displays a three-dimensional (3D) map of the absorption coefficient as a function of cone height and array periodicity, made with a fixed base diameter of 150 nm and a wavelength of 600 nm, which corresponds to the maximum of the AM1.5G solar spectrum. The absorption coefficient increases monotonically with cone height due to an increased optical path length and enhanced multiple scattering within the nanostructure. However, as the height approaches ~700 nm, the growth of the absorption coefficient slows significantly and eventually saturates, indicating a practical upper limit for efficient light trapping. Examining the influence of the nanocone base diameter at fixed heights and wavelengths revealed a non-monotonic dependence on reflection, as shown in Figure 4. The data curve exhibits three distinct regions:

- d < t: An elevated reflection level is observed due to the small effective scattering area and the presence of significant flat substrate regions between sparse cones. These flat areas have a high refractive index and dominate the overall Fresnel reflection.
- d~t: The minimum reflection coefficient is achieved in this region. This corresponds to the regime of dense nanostructure packing, where the most uniform and smooth gradient of the effective refractive index from air to silicon is formed. This ensures efficient reflection suppression.
- d > t: A further increase in diameter degrades the antireflective performance as the nanostructure approaches a quasi-continuous rough layer. This effectively reduces the optical height of the cones.

Overall, the modeling quantitatively identified the relative contribution of each geometric parameter and established criteria for optimizing b-Si design. The results indicate that achieving strong, broadband antireflective performance requires nanocone heights of at least 650 nm, combined with dense packing conditions in which the base diameter approximates the periodicity.

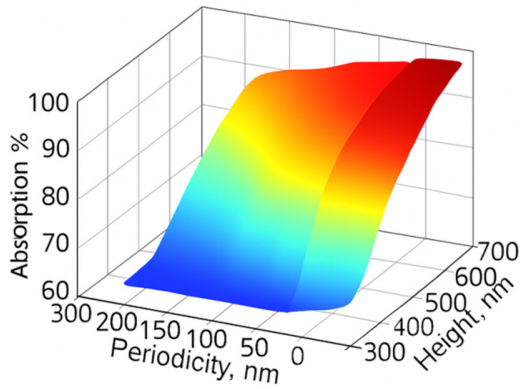

Fig. 3. 3D map of the absorption coefficient as a function of cone height and nanostructure periodicity.

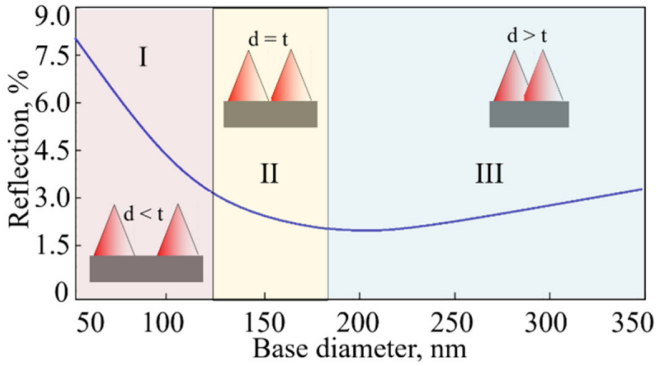

Fig. 4. Dependence of the reflection coefficient on the base diameter of the nanocones.

B. Experimental Investigation

Table I outlines the geometric parameters of b-Si nanoneedles synthesized at etching times of 3 min, 10 min, and 15 min. These parameters include height (h), base diameter (d), lattice periodicity (t), and average sidewall inclination angle (θ) and were measured using SEM analysis. The results confirm that these etching durations correspond to average nanostructure heights of approximately 335 nm, 670 nm, and 765 nm, respectively. As expected, increased etching time results in a deeper, more developed nanostructured b-Si layer.

TABLE I. GEOMETRIC PARAMETERS OF NANONEEDLES

Etching time (min)	***h* (nm)**	***d* (nm)**	***t* (nm)**	**θ (degree)**
3	335±32	167±14	175±21	~14
10	670±58	164±16	179±18	~7
15	765±61	154±19	181±25	~6

Figure 5 shows the absorption, reflectance, and transmittance spectra of b-Si layers that were synthesized by RIE at etching times of 3 min, 10 min, and 15 min. Reflectance and transmittance spectra were measured directly, while absorption was calculated using (1).

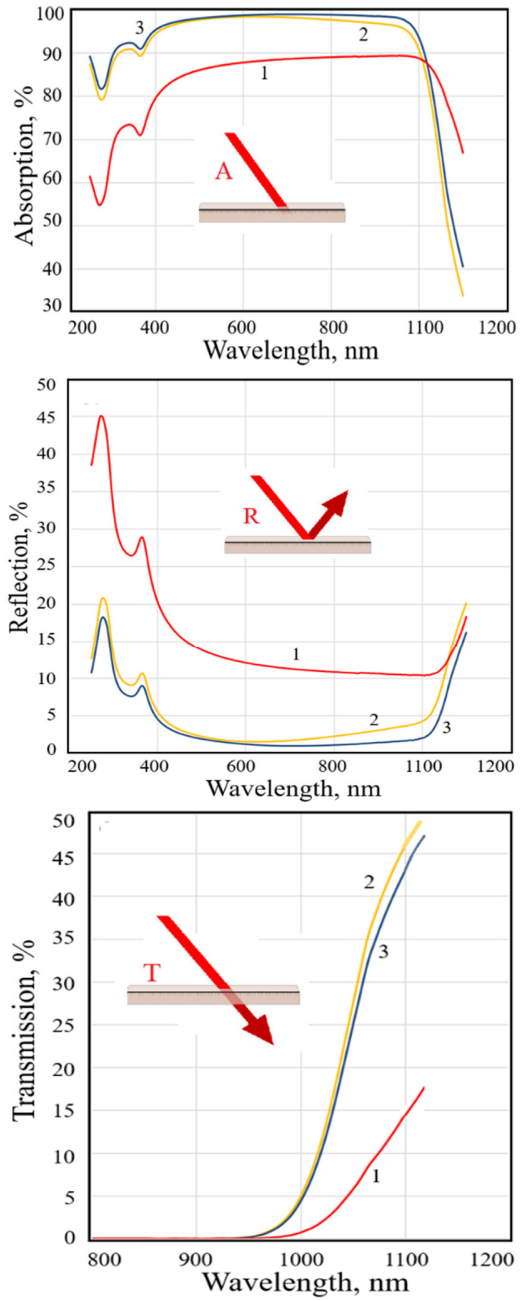

Fig. 5. (a) Absorption, (b) reflection, and (c) transmission spectra of b-Si layers with different nanoneedle heights: 1 - 335 nm, 2 - 670 nm, 3 - 765 nm.

Spectral measurements reveal the significant impact of surface morphology on the optical response. Samples with nanoneedle heights of 670 nm and 765 nm exhibit significantly reduced reflectance and higher absorption across a broad spectral range compared to the sample etched for only three minutes, as portrayed in Figures 5 (a) and (b). This improvement is especially evident in the visible spectrum (400–700 nm), which is crucial for silicon photovoltaic applications due to the high photon flux within this wavelength range. Interestingly, the sample with shorter nanoneedles exhibits comparatively higher absorption in the near-infrared region above ~1100 nm. This behavior is primarily due to silicon's intrinsic optical response: long-wavelength photons have significantly greater penetration depths and are absorbed deep within the bulk material rather than in the nanostructured surface layer. It is also important to note that increasing the nanostructure height from 670 nm to 765 nm only slightly improves the optical properties. This aligns with the saturation behavior predicted by numerical simulations, in which further elongation of nanoneedles yields diminishing returns in light-trapping efficiency. The spectra also exhibit prominent features in the ultraviolet region (250–400 nm), most notably peaks near 270 nm and 360 nm. These peaks correspond to direct interband transitions at critical points in the electronic band structure of crystalline silicon. At longer wavelengths approaching silicon's indirect bandgap energy (~1.1 eV), absorption drops sharply and transmittance increases. This reflects silicon's transition from absorbing to transparent in the near-infrared spectrum.

C. Discussion

Comparing the FDTD modeling results with the experimental measurements shows strong qualitative agreement and acceptable quantitative consistency (6-8%). This confirms that the periodic conical approximation is suitable for describing the optical behavior of b-Si. Minor discrepancies between the regular model and the experiment arise from differences between the idealized geometry and the actual nanostructure morphology. Real b-Si surfaces exhibit variations in cone height, base diameter, taper angle, and local density, as well as structural imperfections, such as agglomerations, partially etched regions, and nanoscale sidewall roughness. These features introduce additional scattering pathways that the regular model does not capture and may slightly alter the effective refractive index profile. The effective refractive index profile of the b-Si layer can be described using Effective Medium Theory (EMT), which applies when the characteristic dimensions of the nanostructures are significantly smaller than the wavelength of the incident light. In this approximation, the nanostructured surface is treated as a depth-dependent composite medium consisting of silicon and air. For b-Si represented as an array of nanocones, this gradient can be described as [17]:

$$n(z) = \left[f(z)n_{Si}^{q} + 1 - f(z)\right]^{1/q} \quad (2)$$

where n_{Si} is the refractive index of bulk silicon, $f(z)$ is the local material filling fraction at depth z, and q=2/3 corresponds to the Bruggeman effective-medium approximation. The filling fraction, $f(z)$, is determined by the nanocone geometry and increases monotonically from the tip of the cone toward its base. Near the top of the nanostructured layer, the silicon volume fraction is small and the effective refractive index is close to that of air. Deeper into the structure, however, the increasing cone cross-section leads to a gradual rise in $f(z)$ and $n(z)$ toward the bulk silicon value. This continuous refractive-index gradient creates a smooth optical transition between air and silicon, which significantly reduces Fresnel reflections at the interface. Rather than encountering a single abrupt refractive-index jump, the incident electromagnetic wave passes through a series of infinitesimal impedance-matched

layers. This results in broadband suppression of reflection and enhanced light coupling into the substrate. Additionally, the graded index profile combined with lateral scattering induced by the nanocone sidewalls increases the effective optical path length within the silicon, further enhancing absorption across a wide spectral range. As the nanocone height increases, the filling-fraction profile becomes smoother and extends over a larger vertical interval. This creates a continuous transition from n=1 (air) to $n_{Si} \approx 3.4$. This gradual change minimizes Fresnel reflections at each interface, resulting in a reduction of total reflectance across the spectrum. Additionally, enlarging the base diameter of the cones increases the local filling fraction, $f(z)$, thereby reducing the amount of exposed flat silicon that would otherwise act as strong Fresnel reflectors. Larger-diameter cones also enhance lateral scattering, redirecting incident light into oblique trajectories and increasing the probability of absorption within the silicon substrate. These mechanisms collectively explain the observed decrease in reflectance with increasing base diameter, up to the point where excessive enlargement leads to partial cone merging, which can ultimately degrade optical performance. The analysis of geometric parameters reveals two dominant optimization factors. First, nanocone height plays a decisive role in light trapping. While extremely tall, high-aspect-ratio nanoneedles may further reduce reflectance, they introduce practical fabrication challenges, such as mechanical fragility, processing instability, and difficulty applying subsequent passivation or protective coatings [18], as well as susceptibility to deformation or collapse during chemical and thermal post-processing [19]. Therefore, the optimal morphology must balance optical performance with manufacturability and long-term reliability. Second, structural density, which is quantified by the relationship between the base diameter (d) and the lattice periodicity (t), plays a critical role. Maximum absorption and minimum reflectance are achieved when $d \sim t$, which corresponds to densely packed nanocones with a minimal amount of planar silicon surface remaining exposed. This configuration ensures the most uniform effective-medium transition and maximizes the scattering-induced enhancement of the optical path length. Although deep RIE enhances light trapping and forms a graded refractive-index profile, improving optical absorption, it also increases the surface area of b-Si. This increase in surface area may lead to enhanced surface recombination and degradation of the electrical performance of silicon solar cells, despite the optical gains. This trade-off can be reduced by creating a protective layer on the b-Si nanostructures using thin films of metal oxides [16, 20]. In summary, the combined modeling and experimental results indicate that nanocone heights of 650–700 nm, together with dense packing where $t/d \sim 1$, constitute the optimal configuration for achieving high-efficiency, broadband antireflection in b-Si. These findings establish clear design criteria for advanced antireflective surfaces and highlight b-Si's substantial potential for improving solar cell and other optoelectronic device performance.

IV. CONCLUSION

This study examined the optical behavior of of black Silicon (b-Si) synthesized by Reactive Ion Etching (RIE) through a combined experimental and numerical approach. Finite-Difference Time-Domain (FDTD) simulations based on a periodic conical representation showed strong agreement with experimentally measured absorption, reflectance, and transmittance spectra, validating the model's effectiveness. The analysis revealed that the dominant factor governing broadband antireflective performance is the formation of a smooth, effective refractive index gradient that becomes increasingly optimized as the nanocone height increases. Simulations and experiments indicate that heights in the range of 650–700 nm provide a practical optimum; beyond this range, additional height results in only marginal improvement. Dense structural packing, characterized by a base-diameter-to-period ratio close to unity, was identified as the second essential parameter for minimizing b-Si reflectance. These results establish clear geometric design principles for maximizing broadband absorption and can be directly applied to optimizing silicon solar cells, photodetectors, and other optoelectronic devices that require efficient broadband antireflection.

ACKNOWLEDGMENT

This work was supported by the Science Committee of the Republic of Armenia (research project no. 21AG-2B011).

REFERENCES

[1] S. Manzoor, M. Filipič, A. Onno, M. Topič, and Z. C. Holman, "Visualizing light trapping within textured silicon solar cells," *Journal of Applied Physics*, vol. 127, no. 6, Feb. 2020, Art. no. 063104, https://doi.org/10.1063/1.5131173.

[2] C. Huo, H. Fu, and K.-Q. Peng, "Inverted pyramid structures fabricated on monocrystalline silicon surface with a NaOH solution," *Heliyon*, vol. 10, no. 1, Jan. 2024, Art. no. e23871, https://doi.org/10.1016/j.heliyon.2023.e23871.

[3] C. Ji *et al.*, "Recent Applications of Antireflection Coatings in Solar Cells," *Photonics*, vol. 9, no. 12, Dec. 2022, Art. no. 906, https://doi.org/10.3390/photonics9120906.

[4] N. Shanmugam, R. Pugazhendhi, R. Madurai Elavarasan, P. Kasiviswanathan, and N. Das, "Anti-Reflective Coating Materials: A Holistic Review from PV Perspective," *Energies*, vol. 13, no. 10, Jan. 2020, Art. no. 2631, https://doi.org/10.3390/en13102631.

[5] V. M. Rotshteyn, T. K. Turdaliev, and Kh. B. Ashurov, "On the Question of the Possibility of Using Nanocrystalline Porous Silicon in Silicon-Based Solar Cells," *Applied Solar Energy*, vol. 57, no. 6, pp. 480–485, Dec. 2021, https://doi.org/10.3103/S0003701X21060153.

[6] M. A. Almeshaal, B. Abdouli, K. Choubani, L. Khezami, and M. B. Rabha, "Study of Porous Silicon Layer Effect in Optoelectronics Properties of Multi-Crystalline Silicon for Photovoltaic Applications," *Silicon*, vol. 15, no. 14, pp. 6025–6032, Sept. 2023, https://doi.org/10.1007/s12633-023-02482-8.

[7] H. Khmissi, B. Azeza, M. Bouzidi, and Z. Al-Rashidi, "Investigation of an Antireflective Coating System for Solar Cells based on Thin Film Multilayers," *Engineering, Technology & Applied Science Research*, vol. 14, no. 3, pp. 14374–14379, June 2024, https://doi.org/10.48084/etasr.7375.

[8] G. Ayvazyan, H. Dashtoyan, and L. Hakhoyan, "Wide-Range Wavelength Light Scattering from Black Silicon Layers: Profits for Perovskite/Si Tandem Solar Cells," *Physica Status Solidi (RRL) – Rapid Research Letters*, vol. 19, no. 2, 2025, Art. no. 2400235, https://doi.org/10.1002/pssr.202400235.

[9] Z. Fan *et al.*, "Recent Progress of Black Silicon: From Fabrications to Applications," *Nanomaterials*, vol. 11, no. 1, Jan. 2021, Art. no. 41, https://doi.org/10.3390/nano11010041.

[10] S. Wang, T. Xie, R. Liang, Y. Zhang, F.-J. Ma, D. Payne, G. Scardera, and B. Hoex, "An artificial-intelligence-assisted investigation on the potential of black silicon nanotextures for silicon solar cells," *ACS*

Applied Nano Materials, vol. 5, no. 8, pp. 11636–11647, 2022, https://doi.org/10.1021/acsanm.2c02619.

[11] G. Ayvazyan, L. Hakhoyan, A. Vardanyan, H. Savin, and X. Liu, "Wetting Properties of Black Silicon Layers Fabricated by Different Techniques," *Physica Status Solidi (RRL) – Rapid Research Letters*, vol. 18, no. 8, 2024, Art. no. 2400072, https://doi.org/10.1002/pssr.202400072.

[12] K. Yee, "Numerical solution of initial boundary value problems involving Maxwell's equations in isotropic media," *IEEE Transactions on Antennas and Propagation*, vol. 14, no. 3, pp. 302–307, 1966, https://doi.org/10.1109/TAP.1966.1138693.

[13] Ansys Lumerical FDTD: Simulation of Photonic Components. Ansys, Inc, 2025.

[14] A. Deinega, S. Belousov, and I. Valuev, "Hybrid transfer-matrix FDTD method for layered periodic structures," *Optics Letters*, vol. 34, no. 6, pp. 860–862, 2009, https://doi.org/10.1364/OL.34.000860.

[15] K. Han and C.-H. Chang, "Numerical modeling of sub-wavelength anti-reflective structures for solar module applications," *Nanomaterials*, vol. 4, no. 1, pp. 87–128, 2014, https://doi.org/10.3390/nano4010087.

[16] X. Zhang *et al.*, "Effects of Black Silicon Surface Morphology Induced by a Femtosecond Laser on Absorptance and Photoelectric Response Efficiency," *Photonics*, vol. 11, no. 10, Oct. 2024, Art. no. 947, https://doi.org/10.3390/photonics11100947.

[17] S. Kim, G. S. Jeong, N. Y. Park, and J.-Y. Choi, "Omnidirectional and broadband antireflection effect with tapered silicon nanostructures fabricated with low-cost and large-area capable nanosphere lithography," *Micromachines*, vol. 12, no. 2, 2021, Art. no. 119, https://doi.org/10.3390/mi12020119.

[18] M. Oproescu, A.-G. Schiopu, V. M. Calinescu, V.-G. Iana, N. Bizon, and M. Sallah, "Influence of Supplementary Oxide Layer on Solar Cell Performance," *Engineering, Technology & Applied Science Research*, vol. 14, no. 2, pp. 13274–13282, Apr. 2024, https://doi.org/10.48084/etasr.6879.

[19] T. P. Pasanen, H. S. Laine, V. Vähänissi, K. Salo, S. Husein, and H. Savin, "Impact of Standard Cleaning on Electrical and Optical Properties of Phosphorus-Doped Black Silicon," *IEEE Journal of Photovoltaics*, vol. 8, no. 3, pp. 697–702, Feb. 2018, https://doi.org/10.1109/JPHOTOV.2018.2806298.

[20] T. Rahman, R. S. Bonilla, R. Nawabjan, P. Wilshaw, and S. Boden, "Passivation of all-angle black surfaces for silicon solar cells," *Solar Energy Materials and Solar Cells*, vol. 160, pp. 444–453, 2017, https://doi.org/10.1016/j.solmat.2016.10.044.